Microdroplet identification and size measurement in sprays with lasing images

Ali Serpengüzel, Serkan Küçükşenel
Koç University, Department of Physics, Microphotonics Research Laboratory, Rumeli Feneri Yolu, Sariyer, Istanbul 80910 Turkey
aserpenguzel@ku.edu.tr

Richard K. Chang
Yale University, Department of Applied Physics and Center for Laser Diagnostics, New Haven, Connecticut 06520 USA

Abstract: Two-dimensional fluorescence and lasing images of a Rhodamine-6G doped water spray are observed with color photography. The lasing microdroplets are identified by their two reciprocal lasing spots. The microdroplet sizes are measured using the digitized images. The measured mean microdroplet diameter is 69.7 μm with a standard deviation of 23.1 μm. The measured microdroplet size distribution compares favorably with the normal Gaussian size distribution.
©2002 Optical Society of America
OCIS codes: (010.1100) Aerosol detection; (230.5750) Resonators; (250.5230) Photoluminescence; (300.2530) Laser induced fluorescence.

References and links

1. R. A. Mugele and H. D. Evans: "Droplet Size Distribution in Sprays," Ind. Eng. Chem. **43**, 1317-1324 (1951).
2. M. Q. McQuay, R. K. Dubey, and W. A. Nazeer, "An experimental sturdy on the impact of acoustics and spray quality on the emissions of CO and NO from an ethanol spray flame," Fuel **77**, 425-435 (1998).
3. J. H. Koo and E. D. Hirleman, "Review of Principles of Optical Techniques for Particle Size Measurements," in *Recent Advances in Spray Combustion: Spray Atomization and Drop Burning Phenomena*, K.K. Kuo, Ed. (AIAA, Virginia, 1996). pp. 3-32.
4. G. A. Ruff and G. M. Faeth, "Nonintrusive Measurements of the Structure of Dense Sprays," in *Recent Advances in Spray Combustion: Spray Atomization and Drop Burning Phenomena*, K.K. Kuo, Ed. (AIAA, Virginia, 1996). pp. 263-296.
5. D. J. Holve and S. A. Self, "Optical particle sizing for in-situ measurements: part I," Appl. Opt. **18**, 1632-1645 (1979); D. J. Holve and S. A. Self, "Optical particle sizing for in-situ measurements: part II," Appl. Opt. **18**, 1646-1652 (1979).
6. J. S. Batchelder and M. A. Taubenblatt, "Interferometric detection of forward scattered light from small particles," Appl. Phys. Lett. **55**, 215-217 (1989).
7. M. Golombok, V. Morin, and C. Mounaim-Rousselle, "Droplet diameter and the interference fringes between reflected and refracted light," J. Phys. D: Appl. Phys. **31**, 59-62 (1998).
8. W. D. Bachalo, "Method for measuring the size and velocity of spheres by dual-beam light-scatter interferometry," Appl. Opt. **19**, 363-370 (1980).
9. A. Mansour and N. Chigier, "Air-blast atomization of non-Newtonian liquids," J. Non-Newtonian liquids **58**, 161-194 (1995).
10. D. R. Secker, P. H. Kaye, R. S. Greenaway, E. Hirst, D. L. Bartley, and G. Videen, "Light scattering from deformed droplets and droplets with inclusions. 1. Experimental results," Appl. Opt. **39**, 5023-5030 (2000); G. Videen, W. Sun, Q. Fu, D. R. Secker, R. S. Greenaway, P. H. Kaye, E. Hirst, and D. Bartley, "Light scattering from deformed droplets and droplets with inclusions. 2. Theoretical treatment," Appl. Opt. **39**, 5031-5039 (2000).
11. D. C. Herpfer and San-Mou Jeng, "Planar Measurements of Droplet Velocities and Sizes Within a Simplex Atomizer," AIAA J. **35**, 127-132 (1997).
12. B. D. Stojkovic and V. Sick, "Evolution and impingement of an automotive fuel spray investigated with simultaneous Mie/LIF techniques," Appl. Phys. B **73**, 75-83 (2001).
13. R. A. Dobbins and G. S. Jizmagian, "Particle size measurements based on the use of mean scattering cross sections," J. Opt. Soc. Am. **56**, 1351-1354 (1966).

#1652 - $15.00 US Received September 03, 2002; Revised October 02, 2002

14. R.R. Maly, G.W. Mayer, B. Reck, and R.A. Schaudt, "Optical Diagnostic for Diesel-Sprays with µs-Time Resolution," SAE paper 910727, (1991).
15. N. L. Swanson, B. D. Billard, and T. L. Gennaro, "Limits of optical transmission measurements with application to particle sizing techniques," Appl. Opt. **38**, 5887-5893 (1999).
16. R. A. Dobbins, L. Crocco, and I. Glassman, "Measurement of mean particle sizes of sprays from diffractively scattered light," AIAA J. **1**, 1882-1886 (1963).
17. J. L. Brenguier, T. Bourrianne, A. D. Coelho, J. Isbert, R. Peytavi, D. Trevarin, and P. Weschler, "Improvements of Droplet Size Distribution Measurements with the Fast-FSSP (Forward Scattering Spectrometer Probe)," J. Atmospheric Oceanic Technol. **15**, 1077-1090 (1998).
18. A. V. Korolev, J. W. Strapp, and G. A. Isaac, "Evaluation of the accuracy of PMS optical array probes," J. Atmospheric Oceanic Tech. **15**, 708-720 (1998).
19. T. E. Corcoran, R. Hitron, W. Humphrey, and N. Chigier, "Optical measurement of nebulizer sprays: a quantitative comparison of diffraction, phase Doppler interferometry, and time of flight techniques," J. Aerosol Sci. **31**, 35-50 (1999).
20. T. Thorsen, R. W. Roberts, F. H. Arnold, and S. R. Quake, "Dynamic Pattern Formation in a Vesicle-Generating Microfluidic Device," Phys. Rev. Lett. **86**, 4163-4166 (2001).
21. N. Dombrowski and R. P. Fraser, "A Photographic Investigation into the Disintegration of Liquid Sheets," Phil. Trans. A **247**, 101-130 (1954).
22. H. Malot and J. B. Blaisot, "Droplet size distribution and sphericity measurements of low-density sprays through image analysis," Part. Syst. Charact. **17**, 146-158 (2000).
23. T. Kamimoto, H. Kobayashi, and S. Matsuoka, "A Big Size Rapid Compression Machine for Fundamental Studies of Diesel Combustion," SAE paper 811004 (1981).
24. B. A. Weiss, P. Derov, D. DeBiase, and H. C. Simmons, "Fluid particle sizing using a fully automated optical imaging system," Opt. Eng. **23**, 561-566 (1984).
25. C. R. Tuck, M. C. Butler and P. C. H Miller, "Techniques for measurement of droplet size and velocity distributions in agricultural sprays," J. Crop Protection **7**, 619-628 (1997).
26. K. D. Ahlers and D. R. Alexander, "Microcomputer based digital image processing system developed to count and size laser-generated small particle images," Opt. Eng. **24**, 1060-1065 (1985).
27. A. R. Glover, S. M. Skippon, and R. D. Boyle, "Interferometric laser imaging for droplet sizing: a method for droplet-size measurement in sparse spray systems," Appl. Opt. **34**, 8409-8421 (1995).
28. R. Albert and P. V. Farrell, "Droplet sizing using the Shifrin inversion," J. Fluids Engineering **116**, 357-362 (1994).
29. K.R. Browne, I.M. Partridge, and G. Greeves, "Fuel Property Effects on Fuel/Air Mixing in an Experimental Diesel Engine," SAE paper 860223 (1986).
30. N. Chigier, "Optical Imaging of Sprays," Prog. Energy Combust. Sci. **17**, 211-262 (1991).
31. L. A. Melton and J.F. Verdieck, "Vapor/Liquid Visualization for Fuel Sprays," Combust. Sci. and Tech. **42**, 217-222 (1985).
32. M. C. Jermy and D. A. Greenhalgh, "Planar dropsizing by elastic and fluorescence scattering in sprays too dense for phase Doppler measurement," Appl. Phys. B **71**, 703-710 (2000).
33. W. P. Acker, A. Serpengüzel, R.K. Chang, and S.C. Hill, "Stimulated Raman Scattering of Fuel Droplets: Chemical Concentration and Size Determination," Appl. Phys. B **51**, 9-16 (1990).
34. M. Golombok and D. B. Pye, "Droplet sizing in fuel injections by stimulated Raman scattering," Opt. Lett. **15**, 872-874 (1990).
35. L. A. Melton, "Spectrally Separated Fluorescence Emissions for Diesel Fuel Droplets and Vapor," Appl. Opt. **22**, 2224-2226 (1983).
36. D. A. Gromov, K. M. Dyumaev, A. A. Manenkov, A. P. Maslyukov, G. A. Matyushin, V. S. Nechitailo, and A. M. Prokhorov , "Efficient plastic-host dye lasers," J. Opt. Soc. Am. B, **2**, 1208-1031 (1985).
37. C.-N. Yeh, H. Kosaka, and T. Kamimoto, "Measurement of drop sizes in unsteady dense sprays," in *Recent Advances in Spray Combustion: Spray Atomization and Drop Burning Phenomena*, K.K. Kuo, Ed. (AIAA, Virginia, 1996). pp. 297-308.
38. A. Serpengüzel, J.C. Swindal, R.K. Chang, and W. P. Acker, "Two-dimensional imaging of sprays with fluorescence, lasing, and stimulated Raman scattering," Appl. Opt. **31**, 3543-3551 (1992).
39. Y. Yamamoto, F. Tassone, and H. Cao, *Semiconductor Cavity Quantum Electrodynamics* (Springer-Verlag, New York, 2000).
40. P. R. Berman, Ed., *Cavity Quantum Electrodynamics* (Academic Press, San Diego, 1993).
41. Y. Yamamoto and A. Imamoglu, *Mesoscopic Quantum Optics* (Wiley, New York, 1999).
42. J. Rarity and C. Weisbuch, Eds., *Microcavities and Photonic Bandgaps: Physics and Applications* (Kluver, Dordrecht, 1996).
43. E. M. Purcell, "Spontaneous Emission Probabilities at Radio Frequencies," Phys. Rev. **69**, 681 (1946).
44. P. W. Milloni and P. L. Knight, "Spontaneous emission between mirrors," Opt. Commun. **9**, 119 - 122 (1973).
45. F. De Martini, G. Innocenti, G. R. Jacobowitz, and P. Mataloni, "Anomalous Spontaneous Emission Time in a Microscopic Optical Cavity," Phys. Rev. Lett. **59**, 2955 - 2958 (1987).
46. H. Yokoyama, K. Nishi, T. Anan, H. Yamada, S. D. Brorson, and E. P. Ippen, "Enhanced Spontaneous Emission from GaAs quantum Wells in Monolithic Microcavities," Appl. Phys. Lett. **57**, 2814 - 2816 (1990).

#1652 - $15.00 US Received September 03, 2002; Revised October 02, 2002
(C) 2002 OSA

47. G. Björk, S. Machida, Y. Yamamoto, and K. Igeta, "Modification of spontaneous emission rate in planar dielectric microstructures, Phys. Rev. A **44**, 669 - 681 (1991).
48. M. S. Skolnick, T. A. Fisher, and D. M. Whittaker, "Strong Coupling Phenomena in Quantum Microcavity Structures," Semiconductor Science Technol. **13**, 645 - 669 (1998).
49. Y. Zhu, J. Gauthier, S. E. Morin, Q. Wu, H.J. Carmichael, and T.W. Mossberg, "Vacuum Rabi splitting as a feature of linear dispersion theory: analysis and experimental observations," Phys Rev. Lett. **64**, 2499 - 2502 (1990).
50. C. Weisbuch, M. Nishioka, A. Ishikawa, and Y. Arakawa, "Observation of coupled exciton-photon mode splitting in a semiconductor quantum microcavity," Phys. Rev. Lett. **69**, 3314 - 3317 (1992).
51. S. Pau, G. Björk, J. Jacobson, H. Cao, and Y. Yamamoto, "Microcavity exciton-polariton splitting in the linear regime," Phys. Rev. B **51**, 14437 - 14447 (1995).
52. D. G. Lidzey, D. D. C. Bradley, S. J. Martin, and M. A. Pate, "Pixelated multicolor microcavity displays," IEEE J. Sel. Top. Quantum Electron. **4**, 113 (1998).
53. H. Yokoyama and K. Ujihara, Eds., *Spontaneous emission and laser oscillation in microcavities* (CRC Press, Boca Raton, 1995).
54. M. S. Ünlü and S. Strite, "Resonant Cavity Enhanced Photonic Devices," J. Appl. Phys. **78**, 607 (1995).
55. H. Benisty, H. De Neve, and C. Weisbuch, "Impact of Planar Microcavity Effects on Light Extraction - Part I: Basic Concepts and Analytical Trends," IEEE J. Sel. Top. Quantum Electron. **34**, 1612 (1998); H. Benisty, H. De Neve, and C. Weisbuch, "Impact of Planar Microcavity Effects on Light Extraction - Part II: Selected Exact Simulations and Role of Photon Recycling," IEEE J. Sel. Top. Quantum Electron. **34**, 1632 (1998).
56. R. E. Slusher and C. Weisbuch, "Optical microcavities in condensed matter systems," Solid State Commun. **92,** 149 (1994).
57. E. F. Schubert, Y.-H. Wang, A. Y. Cho, l. W. Tu, and G. J. Zydzik, "Resonant Cavity Light Emitting Diode," Appl. Phys. Lett. **60**, 921 (1992).
58. H. Yokoyama, K. Nishi, T. Anan, Y. Nambu, S. D. Brorson, E. P. Ippen, and M. Suzuki, "Controlling spontaneous emission and threshold-less laser oscillation with optical microcavities," Opt. Quantum Electron., **24**, S245 (1992).
59. Y. Yamamoto, S. Machida, and G. Björk, "Microcavity semiconductor laser with enhanced spontaneous emission," Phys. Rev A **44,** 657 (1991).
60. J.V. Sandusky and S. R. J. Brueck, "Observation of spontaneous emission microcavity effects in an external-cavity surface emitting laser structure," Appl. Phys. Lett. **69**, 3993 (1996).
61. S. L. McCall, A. F. J. Levi, R. E. Slusher, S. J. Pearton, and R. A. Logan, "Whispering Gallery Mode Microdisk Lasers," Appl. Phys. Lett. **60**, 289 (1992).
62. J. P. Zhang, D. Y. Chu, S. L. Wu, S. T. Ho, W. G. Bi, C. W. Tu, and R. C. Tiberio, "Photonic Wire Laser," Phys. Rev. Lett. **75**, 2678 (1995).
63. R. K. Chang and A. J. Campillo, Eds., *Optical Processes in Microcavities* (World Scientific, Singapore, 1996).
64. P. W. Barber and R. K. Chang, Eds., *Optical Effects Associated With Small Particles* (World Scientific, Singapore, 1988).
65. A. Ashkin and J. M. Dziedzic, " Observation of Resonances in the Radiation Pressure on Dielectric Spheres," Phys. Rev. Lett. **38**, 1351-1354 (1977).
66. R. K. Chang, "Micrometer-Size Droplets as Optical Cavities: Lasing and Other Non-linear Effects," in *Advances in Laser Science-II*, M. Lapp, W. C. Stwalley, and G. A. Kenny-Wallace, Eds. (American Institute of Physics, New York, 1987). pp. 509-515.
67. R. E. Benner, P. W. Barber, J. F. Owen, and R. K. Chang, "Observation of Structure Resonances in the Fluorescence Spectra from Microspheres," Phys. Rev. Lett. **44**, 475-478 (1980).
68. D. S. Benincasa, P. W. Barber, J. -Z. Zhang, W. -F. Hsieh, and R.K. Chang, "Spatial Distribution of the Internal and Near-Field Intensities of Large Cylindrical and Spherical Scatterers," Appl. Opt. **26**, 1348-1356 (1987).
69. S. C. Ching, H. M. Lai, and K. Young, "Dielectric Microspheres as Optical Cavities: Thermal Spectrum and Density of States," J. Opt. Soc. Am. B **4**, 1995-2003 (1987).
70. S.-X. Qian, J.B. Snow, H.-M. Tzeng, and R.K. Chang, "Lasing Droplets: Highlighting the Liquid-Air Interface by Laser Emission," Science **231**, 486-488 (1986).
71. P. W. Barber and S. C. Hill, *Light Scattering by Particles: Computational Methods* (World Scientific, Singapore, 1990).
72. S. C. Hill, and R. E. Benner, "Morphology-Dependent Resonances associated with Stimulated Processes in Microspheres," J. Opt. Soc. Am. B **3**, 1509-1514 (1986).
73. J. -Z. Zhang, D. H. Leach, and R. K. Chang, "Photon Lifetime within a Droplet: Temporal Determination of Elastic and Stimulated Raman Scattering," Opt. Lett. **13**, 270-272 (1988).
74. P. R. Conwell, C. K. Rushforth, R. E. Benner, and S. C. Hill, "Efficient Automated Algorithm for the Sizing of Dielectric Microspheres using the Resonance Spectrum," J. Opt. Soc. Am. A **1**, 1181-1186 (1984).
75. H. -B. Lin, J. D. Eversole, and A. J. Campillo, "Identification of Morphology Dependent Resonances in Stimulated Raman Scattering from Microdroplets," Opt. Commun. **77**, 407-410 (1990).
76. E. J. Davis and G. Schweiger, *The Airborne Microparticle: Its Physics, Chemistry, Optics, and Transport Phenomena* (Springer, Berlin, 2002). pp. 350-351.

#1652 - $15.00 US Received September 03, 2002; Revised October 02, 2002
(C) 2002 OSA

77. A. S. Kwok, C. F. Wood, and R. K. Chang, "Fluorescence Imaging of CO_2 Laser-Heated Droplets," Opt. Lett. **15**, 664-666 (1990).
78. R. C. Pfaffenberger and J. H. Patterson, *Statistical Methods for Business and Economics* (Irwin, Illinois, 1987). pp. 1025-1032.
79. J. Benjamin and C. Cornell, *Probability, Statistics, and Decision for Civil Engineers* (McGraw-Hill, New York, 1970). pp. 478-480.

1. Introduction

Sprays are ubiquitous in today's high technology world; and are used in numerous industries, such as medicine, automotive, aerospace, and agriculture. In automotive and aerospace, fuel sprays are important for the combustion process. In automotive engines, hollow-cone nozzle injectors are used to introduce the spray into the combustion chamber.

The constituents of a spray emerging from a nozzle are both in the vapor and the liquid phase. The liquid phase consists of three components: ligaments, small droplets, and large droplets. The spray diverges as it leaves the nozzle, and forms liquid ligaments. These ligaments subsequently break-up into microdroplets, which evaporate as the air entrainment into the diverging spray increases. The relative vapor/liquid composition of the spray is critical to the operation of an internal combustion engine (ICE). Break-up length, penetration depth, spray angle, and the size and spatial distribution of the microdroplets are all important characteristics of the sprays [1]. Particularly, the ignition delay in Diesel engines is dependant on the microdroplet size and number density, i.e., microdroplet size distribution of the spray. Additionally, the carbon monoxide and nitrous oxide emissions from ICE's are found to be dependent on the spray microdroplet size distribution [2].

2. Microdroplet and spray imaging and microdroplet sizing

Various one- and two-dimensional in-situ and non-intrusive optical techniques have been applied for individual microdroplet and spray imaging and microdroplet sizing [3-4]. One-dimensional in-situ techniques such as intensity deconvolution, [5] interferometric phase shift, [6] interferometric imaging, [7] phase Doppler interferometry, [8-9] elastic light scattering, [10-11], and Mie scattering, [12] techniques are limited to single microdroplet measurements, whereas extinction, [13-14] absorption, [15] multiple angle elastic light scattering, [16-17] and Fraunhofer diffraction [18-19] are applicable to spray measurements. Fraunhofer diffraction is the most commonly used one-dimensional microdroplet size measurement technique, and is capable of a resolution of 1 μm with a collection lens of 100 mm focal length in dilute sprays. Two dimensional in-situ elastic imaging techniques such as direct photography, [20] flashlamp illumination, [21-22] backlighting, shadowgraph, [23] direct laser imaging, [24-25], digital image processing, [26] interferometric imaging, [27] Shifrin inversion, [28] Schlieren, [29] and holography [30] are suitable for dilute spray characterization. For the study of dense sprays, two-dimensional in-situ inelastic imaging techniques such as two color exciplex imaging (TCEI), [31] laser induced fluorescence (LIF), [32] lasing, and stimulated Raman scattering (SRS) [33-34] are required.

In the elastic scattering images of the spray, it is not possible to distinguish the vapor and liquid phases or the components of the liquid phase. TCEI is capable of differentiating between the vapor and the liquid phases of the spray [35]. In order to also make LIF phase sensitive, LIF emission from the vapor phase can be eliminated by selecting a dye, which has a low concentration, and poor quantum efficiency in the vapor phase. Rhodamine 6G, being an ionic dye molecule, has a low vapor pressure, and poor quantum efficiency in air, whereas it has a high quantum efficiency of 0.9, when dissolved in a liquid [36]. Consequently, when Rhodamine 6G is added to the liquid emerging from the nozzle, the LIF image is mainly from the liquid ligaments and microdroplets in the spray. The lasing emission from larger

#1652 - $15.00 US Received September 03, 2002; Revised October 02, 2002
(C) 2002 OSA

microdroplets is red shifted relative to the LIF emission. In both TCEI and LIF the droplet size is estimated from the ratio of the fluorescence intensity to the Mie scattering intensity [37]. However, in lasing (or SRS) [38] the microdroplet size can be directly measured form the separation of the two reciprocal lasing (or SRS) spots, without the necessity for additional Mie scattering measurements. Lasing requires much lower input laser intensities compared to SRS, and therefore is less susceptible to multiple scattering of the incident laser intensity. In this paper, we report, for the first time, to our knowledge, the sizing of the microdroplets in a hollow-cone nozzle spray using the lasing images of microdroplets doped with Rhodamine 6G dye.

3. Microcavity Electrodynamics

The microdroplets are perfect optical microcavities. Therefore, we have to understand the unique optical properties of the microcavities. First, the microcavity acts as an optical resonator for light rays with specific wavelengths, which after one round trip, return to their starting position in phase, i.e., resonate in the microcavity [39-40]. This optical feedback is responsible for the observation of nonlinear optical processes, such as lasing (or SRS), in optically transparent microdroplets. For the lasing (or SRS) to occur in a microdroplet, the roundtrip gain has to be bigger than the roundtrip loss. When the microdroplet liquid is not optically transparent, e.g. paint, ink, or oil suspensions in water as in the case of insecticide sprays, the roundtrip gain will be less than the roundtrip loss, and lasing (or SRS) will not occur in the microdroplet. In that case, a substitute transparent liquid with the same mechanical properties doped with the appropriate laser dye can be used for spray characterization.

Second, in a microcavity, the photon density of states (DOS) are enhanced at the cavity resonances, when compared with the continuum of photon states of a bulk sample. The spontaneous emission (luminescence) cross-sections (quantum efficiencies) at the microcavity resonances are larger than the bulk spontaneous emission cross-sections because of the enhanced photon DOS [41]. This brings the additional possibility to control the emission properties of materials [42]. The cavity alteration of the spontaneous emission was first proposed for radio waves [43]. Afterwards, the microcavity alteration of the spontaneous emission was proposed [44] and observed in organic microcavities, [45] in the optical part of the electromagnetic spectrum. In addition, alteration of the spontaneous emission in semiconductor microcavities was observed [46] and calculated [47].

There are two coupling regimes between the microcavity photon modes and the gain media modes (e.g., excitons): weak coupling and strong coupling. In this weak coupling regime, the interaction (Rabi coupling) strength is smaller than the microcavity mode damping (linewidth) and the gain media mode (e.g., exciton) damping (linewidth). The spontaneous emission spectrum is altered due to a redistribution of the DOS by the presence of the microcavity. However, in the strong coupling regime, the interaction (Rabi coupling) strength is bigger than the microcavity mode damping (linewidth) and gain media mode (e.g., excitons) damping (linewidth), and Rabi splitting of the microcavity and gain media mode (e.g., excitons) occurs [48]. The proposition of strong coupling in optical microcavities, [49] was followed by its experimental observation [50] and theoretical calculation [51].

Optical microcavities can now be realized in solid state systems such as organic materials [52] and semiconductors [53]. Semiconductor microcavities are used in resonant cavity enhanced (RCE) optoelectronic devices, which are wavelength selective and ideal for dense wavelength division multiplexing (DWDM) applications [54]. The simple planar Fabry-Perot resonator is the most widely used geometry in semiconductor microcavities [55]. As they alter the optoelectronic properties of the photonic gain media, semiconductor

#1652 - $15.00 US Received September 03, 2002; Revised October 02, 2002
(C) 2002 OSA

microcavities can be used in very efficient light emitting diodes (LED's), [56] in RCE LED's, [57] in low threshold vertical cavity surface emitting lasers (VCSEL's), [58-59] external-cavity surface emitting lasers, [60] microdisk, [61] and microwire [62] lasers.

4. Microdroplet Electrodynamics

The occurrence of lasing in relatively large microdroplets can be explained by examining the electromagnetic and quantum electrodynamic (QED) properties of the microdroplets [63]. Because of the spherical liquid-air interface, a third effect can occur in a large microdroplet in addition to the previously mentioned optical effects, i.e., optical cavity feedback, and enhanced cross section. For a plane wave illumination, the internal input intensity is concentrated in two small regions along the principal diameter. This intensity magnification can be as high as 100 times just within the microdroplet shadow face, and 10 times just within the microdroplet illuminated face, [64] and reduces the threshold of nonlinear optical processes. Figure 1 shows the schematic of the equatorial plane of the microdroplet.

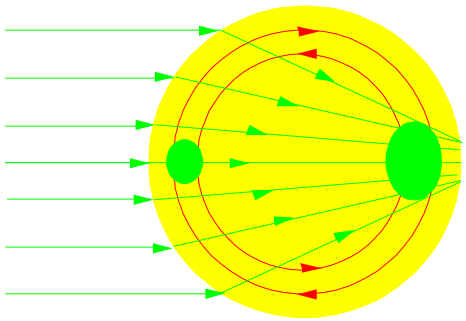


Fig. 1. The schematic of the equatorial plane of the microdroplet showing the focusing effect of the microdroplet with high intensity pump regions and the counter-propagating morphology dependent resonances. The pump input laser is shown in green, the fluorescing microdroplet is shown in yellow, and the counterpropagating and lasing MDR's are shown in orange-red. The two high intensity spots in the illuminated and shadow side are indicated by green ellipses.

Additionally, as mentioned in the previous section, the microdroplet acts as an optical cavity for specific wavelengths that satisfy the morphology-dependent resonances (MDR's) [65-66]. MDR's are usually treated as standing waves, which can be decomposed into two counterpropagating traveling waves, which propagate around the microdroplet rim [67]. The counterpropagating traveling waves must experience quasi-total-internal reflection (TIR) repeatedly at the spherical microdroplet interface and return to the starting point with their initial phase. For wavelengths that are on MDR's, and within the optical gain profile of the medium, the generated nonlinear waves circulate around the microdroplet rim, and experience gain at the two high internal intensity regions. Occasionally, when the monochromatic input laser frequency, is tuned to a MDR (an input resonance), there can be an even larger enhancement of the internal intensity, which can further reduce the threshold for nonlinear optical effects [68]. Finally, the fluorescence cross sections of molecules in the microdroplets can be larger than those in an optical cell because of the modified final DOS of the quantum mechanical transition probability. In a microdroplet, the final states of the quantum mechanical transition probability are the microdroplet cavity modes (described by MDR's), while for bulk liquid in an optical cell the final states of the transition probability are the continuum modes of an infinite system [69]. These three effects (enhanced internal field, optical cavity feedback, and enhanced cross section) reduce the threshold for nonlinear optical effects, e.g., the lasing threshold for dye-doped microdroplets.

#1652 - $15.00 US Received September 03, 2002; Revised October 02, 2002
(C) 2002 OSA

MDR's are responsible for lowering the intensity thresholds for lasing in fluorescent dye-doped droplets [70]. For spherical microdroplets, the spectral position of the MDR's can be calculated from the Lorenz-Mie theory [71]. The density of MDR's per unit frequency interval [72] is sufficiently large (typically 2 MDR's per cm^{-1} for microdroplets with a radius of 40 μm and a wavelength of 500 nm) that numerous MDR's are spanned by both the fluorescence linewidth (typically 10^3 cm^{-1}). The quality factor of a MDR, defined as the energy stored in the microdroplet cavity divided by the energy lost per cycle, has been calculated to be on the order of 10^8 for a microdroplet with a size parameter of 300, real part of the index of refraction of 1.5, and imaginary part of the index of refraction of 10^{-8}. By measuring the decay time of the SRS leaking from an ethanol microdroplet with a radius of 35 μm after the input beam is shut off, the quality factor is experimentally determined [73] to be on the order of 10^7. Such large quality factors greatly reduce the input intensity needed to achieve the lasing threshold at discrete frequencies corresponding to MDR's within the fluorescence linewidth. Individual lasing peaks at MDR's may be resolved with a moderate-resolution spectrograph (with 1 cm^{-1} resolution). The absolute frequency of the MDR's or, more simply the separation between the MDR-related peaks, provides an accurate measurement of the microdroplet size [74-75].

5. Fluorescence and Lasing in Microdroplets

The lasing wavelengths of laser-dye doped microdroplets are on the red side of the fluorescence maximum. The red shift of the lasing spectrum of microdroplets as well as that of the dye-doped liquids in an optical cell are associated with the increasing dye absorption, which reaches a maximum on the blue side of the fluorescence maximum. The lasing threshold is proportional to the difference between the fluorescence quantum efficiency and the absorption loss. For dyes with small Franck-Condon shifts, the fluorescence maximum and absorption maximum are closely separated. Consequently, for these dyes the lasing wavelength region is significantly red shifted relative to the fluorescence maximum. As the dye concentration is increased, the red shift increases further. Therefore, the radiation from the large microdroplets in the spray, which are more likely to achieve the lasing threshold, is expected to be red shifted relative to the fluorescence from the small microdroplets and liquid ligaments of the spray, which do not achieve the lasing threshold. The Rhodamine 6G dye-doped larger microdroplets are expected to emit orange-red lasing radiation. However, the radiation from the Rhodamine 6G dye-doped liquid ligaments is expected to remain yellow because the shape of the liquid ligaments cannot provide optical feedback for the internally generated fluorescence and/or amplified fluorescence radiation. Again, the vapor phase does not contribute to the radiation because of Rhodamine 6G's low vapor pressure and poor fluorescence quantum efficiency in the vapor phase. From Lorenz-Mie calculations, it is known that the quality factor (Q) of the MDR's decrease as the microdroplet radius decreases and/or the microdroplet index of refraction approaches that of the surrounding medium.

For Rhodamine 6G dye doped water microdroplets with an index of refraction of 1.33, we are uncertain of the size below which the quality factors are too low to support lasing at a fixed input pump intensity. With a stream of monodisperse water microdroplets with radii greater than 20 micrometer and containing Rhodamine 6G, the lasing threshold is achieved with an input pump laser intensity of 0.1 KW/cm^2. Because the smaller microdroplets have lower Q MDR's and less MDR's within the gain profile of the Rhodamine 6G dye, than larger microdroplets, the small microdroplets will only fluoresce, when the input laser intensity is below the lasing threshold intensity. Due to cavity QED considerations, some small droplets will also lase with lower thresholds than the larger microdroplets. However, small droplets have relatively lower chance of lasing, since bigger droplets have more

#1652 - $15.00 US Received September 03, 2002; Revised October 02, 2002
(C) 2002 OSA

MDR's within the gain profile of the Rhodamine 6G dye. The Q's of the MDR's are limited by the absorption coefficient of the water containing 10^{-4} M Rhodamine 6G. The absorption coefficient of Rhodamine 6G is approximately 10^5 M^{-1} cm^{-1}, which results in an absorption coefficient of 10 cm^{-1}, and limits the Q's to 10^3. This reduction of in Q's further limits the number of available MDR's for lasing.

Additionally, a change in dye concentration will also change the lasing threshold in the microdroplets. An increase in the dye concentration will both increase the gain, and the absorption loss in the microdroplets. After the saturation of the gain, a further increase of the concentration will further reduce the Q's. In our system, a uniform dye concentration is assumed for all microdroplets sizes, since the microdroplet evaporation rate is on the order of 100 $\mu m^2/s$ [76]. At our nozzle speeds of 10 m/s, this will not cause a substantial increase in the dye concentration.

6. Experimental Procedure

The lasing and fluorescence images of the spray were obtained using the setup shown in Fig. 2. The illumination source is the second-harmonic output of a multimode Q-switched Nd:YAG laser. The laser has an excitation wavelength of 532 nm, a repetition rate of 10 Hz, and a pulse duration of 15 ns. The laser beam is propagating along a horizontal line with a vertical polarization. The laser beam is formed into a sheet with a length of 10 mm and a thickness of 100 μm using the combination of a diverging spherical lens and a converging cylindrical lens. The green illumination sheet, with an intensity of 0.1 GW/cm^2, intercepts a select portion of the nozzle spray. The hollow-cone nozzle has a flow rate of 6.25 liters/hr at a back pressure of 4.2 Kg/cm^2 and a cone angle of 30˚. A water spray containing 10^{-4} M Rhodamine 6G emerges from the vertically directed nozzle and is photographed with a 35 mm camera. The fluorescence emission spectrum of Rhodamine 6G is in the yellow-orange-red part of the optical spectrum [65]. The spray is imaged through an orange-red filter (Corning 3-66) and recorded on a 1600 ASA color film. The incident pump beam is filtered by the color filter. The photographs were later digitized for image analysis. The ionic Rhodamine 6G is selected because of its poor fluorescence quantum efficiency in the vapor phase and its low vapor pressure [77].

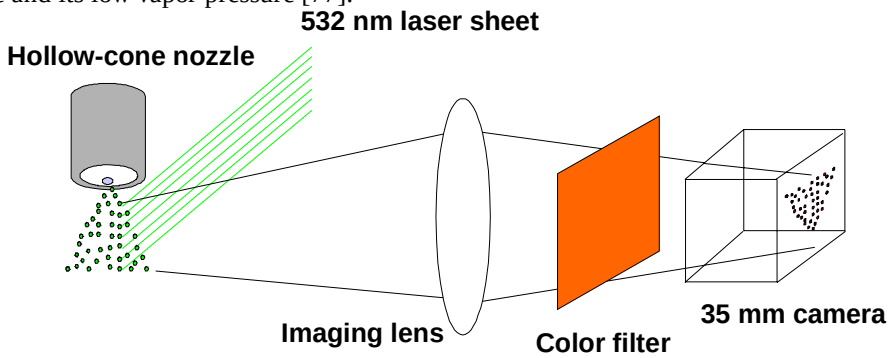


Fig. 2. The experimental setup used to image the spray. A laser sheet illuminates the spray emerging form the hollow-cone nozzle. The spray is imaged through a filter onto the camera.

#1652 - $15.00 US Received September 03, 2002; Revised October 02, 2002
(C) 2002 OSA

7. Microdroplet Imaging with Fluorescence and Lasing

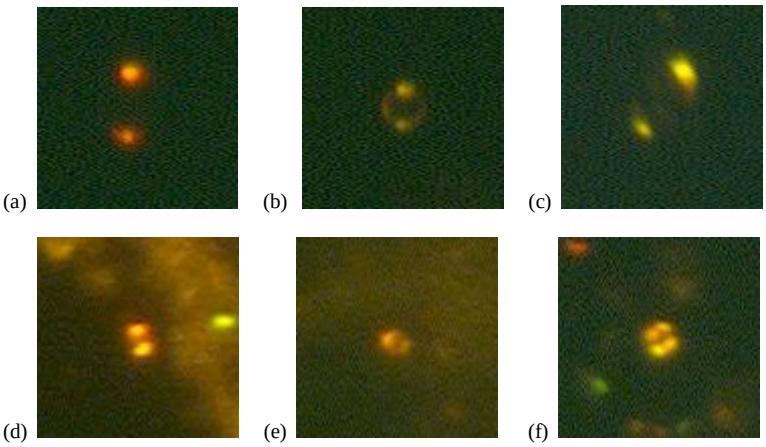


Fig. 3. The experimentally obtained images of the single lasing microdroplets in the (a-c) four times and (b-d) two times magnified images of the Rhodamine-6G doped water spray. Notice the two reciprocal lasing spots corresponding to the two counter-propagating lasing beams. In Fig. 3 (f) there are two sets of perpendicular lasing modes.

In order to interpret the high magnification lasing images of the spray, images of single lasing droplets were investigated. Figure 3 shows images of individual lasing microdroplets. The images shown in Fig. 3 are obtained from a region 1 cm distant from the nozzle orifice. Two reciprocal orange-red dots produced by the lasing radiation, that leaks from the microdroplet rim, is the distinct feature of these images. Experimentally, when the input laser intensity is just above threshold, the lasing appears as two reciprocal small orange-red dots located on the microdroplet rim. The appearance of the two orange-red dots is consistent with the better spatial overlap of the internal pumping region and the MDR's, which are localized around the microdroplet perimeter. The detected radiation from the two orange-red dots is associated with the nonlinear lasing waves, which leak from the microdroplet rim, and are in resonance with MDR's.

8. Spray Imaging with Fluorescence and Lasing

The microdroplet size data is collected from a total of 6 lasing and fluorescing liquid spray images. Four of these images are shown in Figures 4-7 (a). In the images, there is a gradual color variation from yellow to orange to red. The fluorescence is yellow compared to the orange-red lasing, which occurs towards the long wavelength side of the Rhodamine 6G dye gain curve. Only liquid ligaments and small microdroplets appear yellow in the fluorescence image of Rhodamine 6G-doped water spray. Because the large microdroplets achieve the lasing threshold, we are able to distinguish the red-shifted lasing emission of the large microdroplets from the yellow fluorescence emission of small microdroplets and liquid ligaments. Figures 4-7 (b) show the analyzed wavelength-shifted fluorescence and lasing images of the hollow-cone-nozzle spray. The white rectangular boxes depicted in Figs. 4-7 (b) are zoomed in Figs. 4-7 (c) and (d), which show the experimentally obtained and analyzed images, respectively. The lasing microdroplets are selected using the two reciprocal lasing spots corresponding to the two counter-propagating laser beams around the great circles of the microsphere. Each microdroplet is then numbered, and its diameter is measured in pixels, and then converted to spatial units. The size calibration is performed using the magnification of the collection optics and the nozzle size. The result of the size measurements is plotted as a histogram in Fig. 8.

#1652 - $15.00 US Received September 03, 2002; Revised October 02, 2002
(C) 2002 OSA

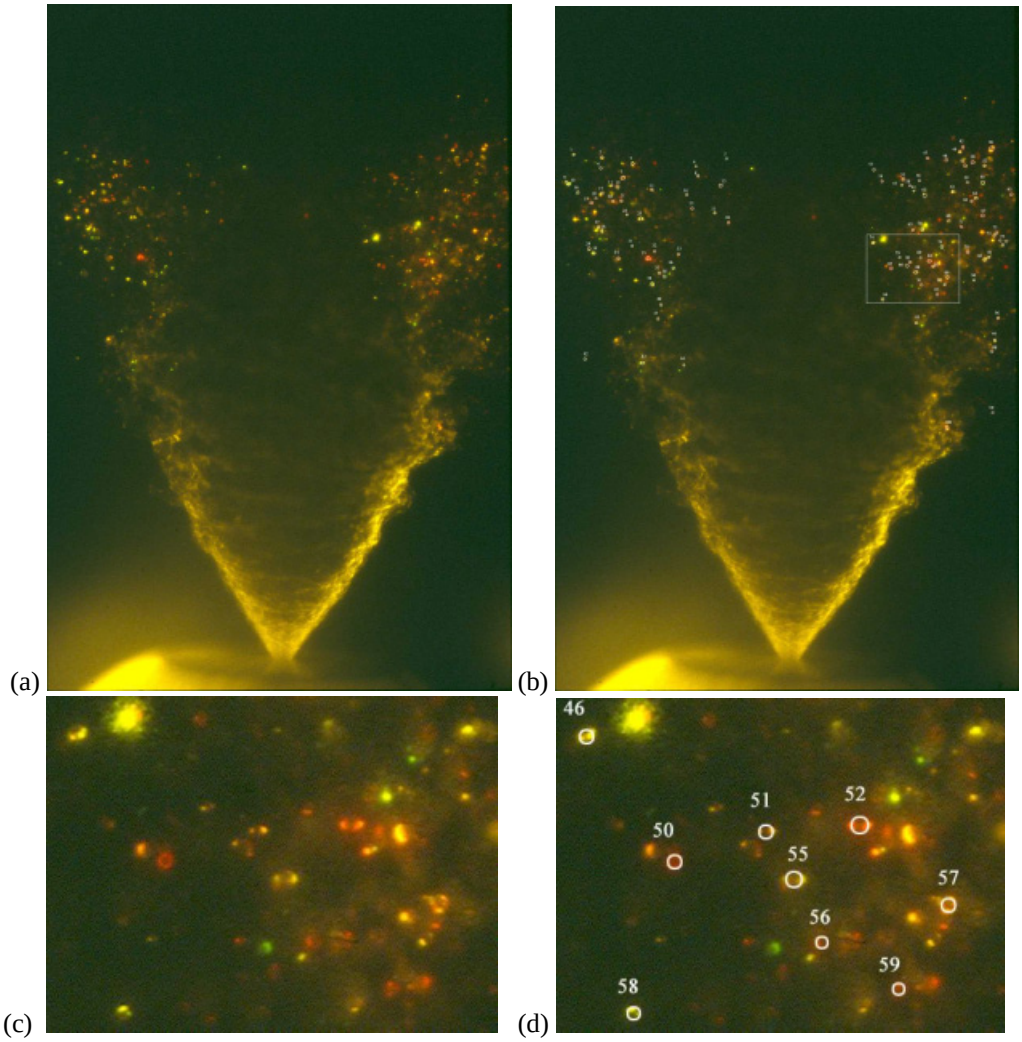


Fig. 4. Experimentally obtained (a) original image and (b) analyzed image of the lasing and fluorescing Rhodamine-6G doped water spray with two times magnification. The white box in (b) indicates the enlarged region shown in (c) and (d). Magnified region of the experimentally obtained (c) original image and (d) analyzed image of the lasing and fluorescing Rhodamine-6G doped water spray. A microdroplet is defined by a pair of reciprocal lasing spots.

The solid red dots in Fig. 8 represent the experimental size measurement data. A Kolmogorov-Smirnov goodness-of-fit test applied to the measured microdroplet size distribution [78-79] satisfied the normality condition. The blue curve in Fig. 8 represents the theoretical fit using the normal Gaussian probability distribution function (PDF) with a mean microdroplet diameter of μ = 69.7 μm and a standard deviation of σ = 23.1 μm. The obtained PDF compares favorably with the theoretical normal Gaussian PDF. The normal Gaussian PDF is given as p(x).

$$p(x) = \frac{1}{\sigma\sqrt{2\pi}} \exp\left(-\frac{1}{2}\left(\frac{d-\mu}{\sigma} \right)^2 \right). \quad (1)$$

#1652 - $15.00 US
Received September 03, 2002; Revised October 02, 2002
(C) 2002 OSA

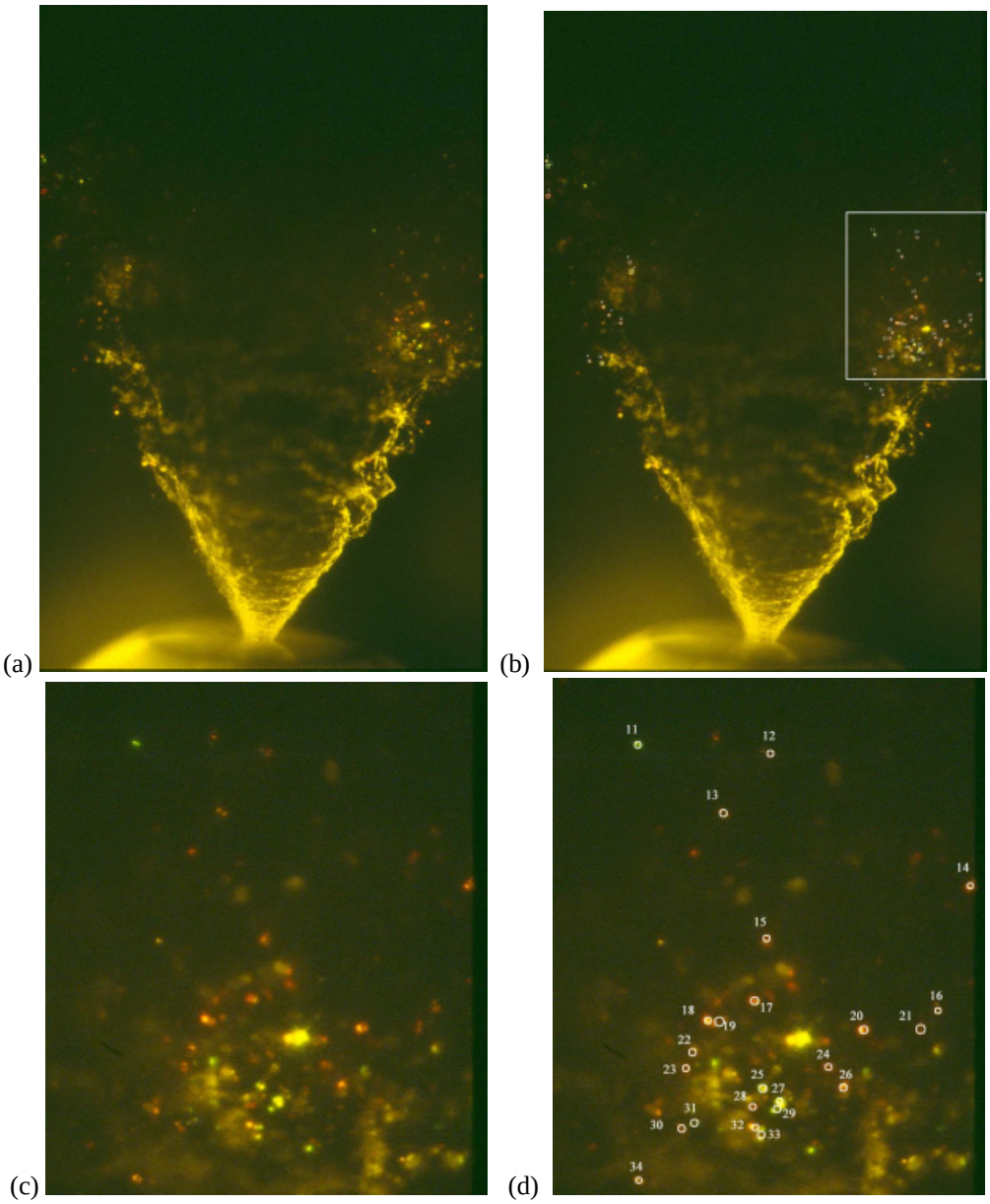


Fig. 5. Experimentally obtained (a) original image and (b) analyzed image of the lasing and fluorescing Rhodamine-6G doped water spray with two times magnification. The white box in (b) indicates the enlarged region shown in (c) and (d). Magnified region of the experimentally obtained (c) original image and (d) analyzed image of the lasing and fluorescing Rhodamine-6G doped water spray. A microdroplet is defined by a pair of reciprocal lasing spots.

where **d** is the microdroplet diameter, **μ** the mean microdroplet diameter, **σ** the standard deviation of the microdroplet diameter. The normal Gaussian PDF can be integrated to yield the normal Gaussian cumulative distribution function (CDF) *F(x).*

#1652 - $15.00 US
Received September 03, 2002; Revised October 02, 2002
(C) 2002 OSA

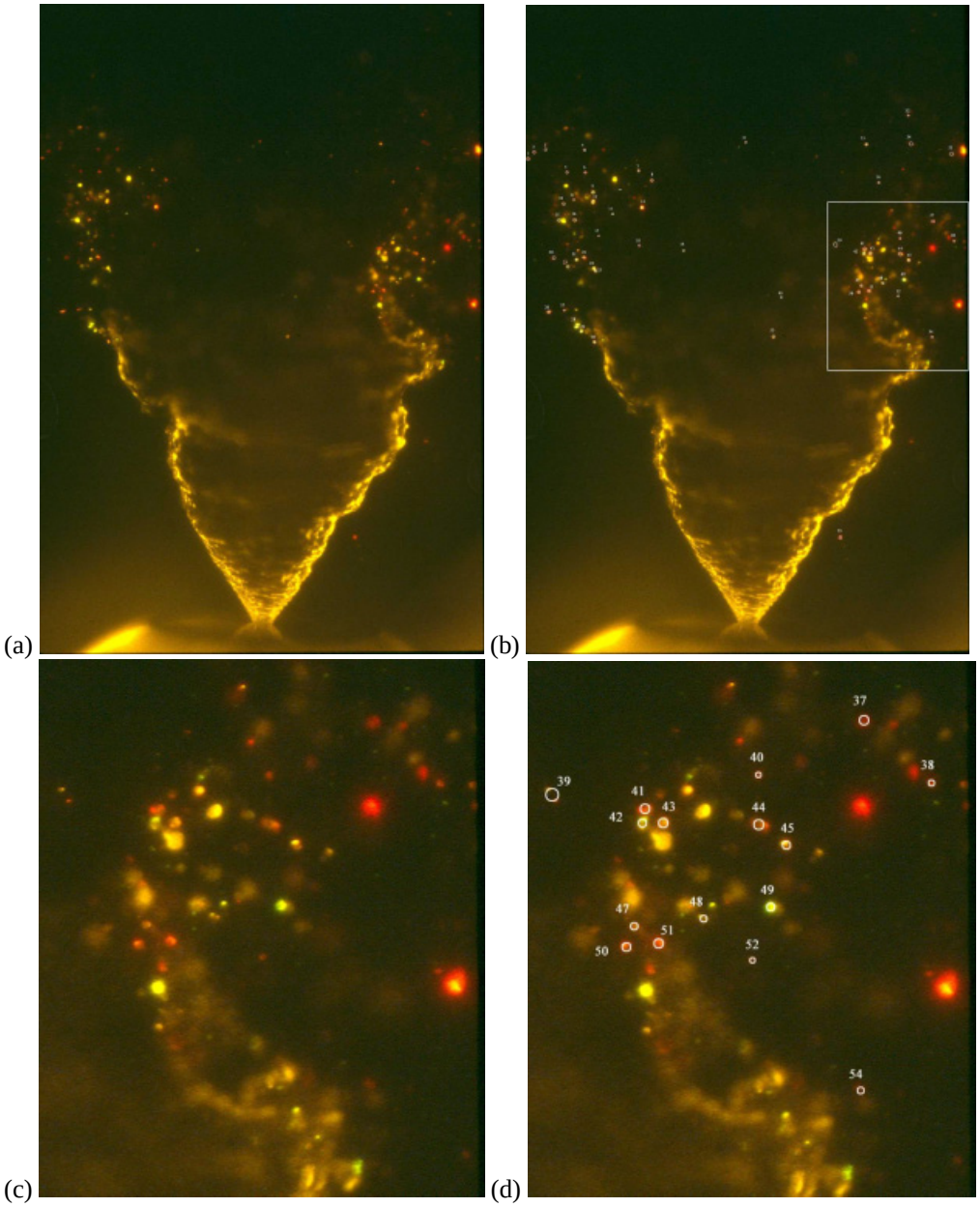


Fig. 6. Experimentally obtained (a) original image and (b) analyzed image of the lasing and fluorescing Rhodamine-6G doped water spray with two times magnification. The white box in (b) indicates the enlarged region shown in (c) and (d). Magnified region of the experimentally obtained (c) original image and (d) analyzed image of the lasing and fluorescing Rhodamine-6G doped water spray. A microdroplet is defined by a pair of reciprocal lasing spots.

$$F(x)=\frac{1}{\sigma\sqrt{2\pi}}\int_{-\infty}^{+\infty}\exp\left(-\frac{1}{2}\left(\frac{d-\mu}{\sigma}\right)^{2}\right)dx\cdot \tag{2}$$

#1652 - $15.00 US
Received September 03, 2002; Revised October 02, 2002
(C) 2002 OSA

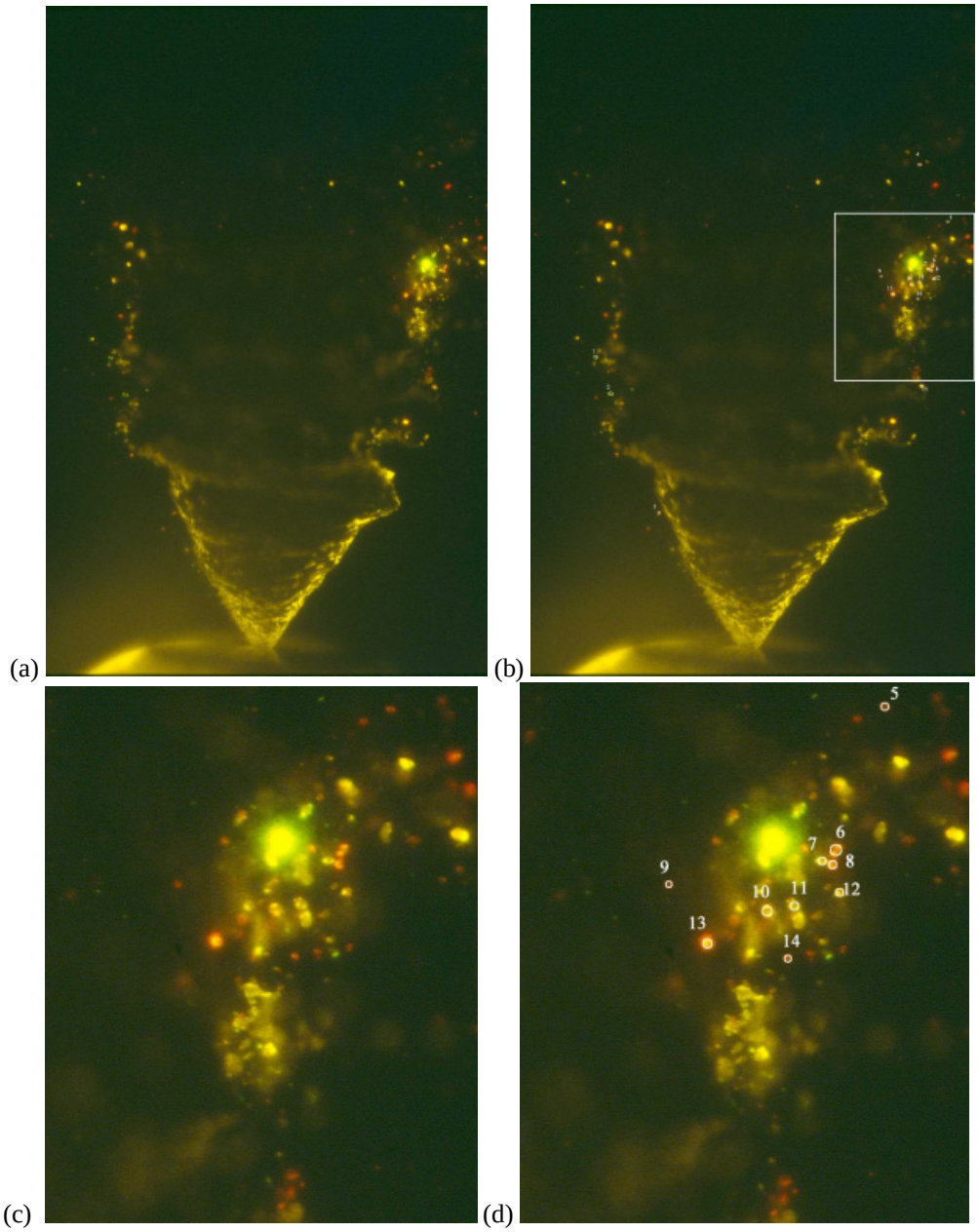


Fig. 7. Experimentally obtained (a) original image and (b) analyzed image of the lasing and fluorescing Rhodamine-6G doped water spray with two times magnification. The white box in (b) indicates the enlarged region shown in (c) and (d). Magnified region of the experimentally obtained (c) original image and (d) analyzed image of the lasing and fluorescing Rhodamine-6G doped water spray. A microdroplet is defined by a pair of reciprocal lasing spots.

The CDF is plotted in Fig. 9 for our microdroplet size distribution. Again, the solid red dots represent the experimental cumulative number of microdroplets, and the blue curve represents the theoretical normal Gaussian CDF. The obtained CDF compares favorably with the theoretical normal Gaussian CDF.

#1652 - $15.00 US Received September 03, 2002; Revised October 02, 2002
(C) 2002 OSA

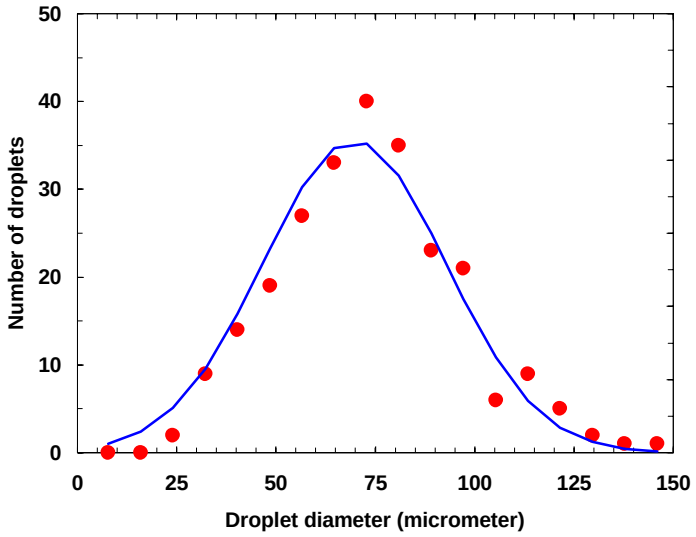


Fig. 8. The histogram plot of the number of microdroplets and the respective normal Gaussian fit as a function of the microdroplet diameter.

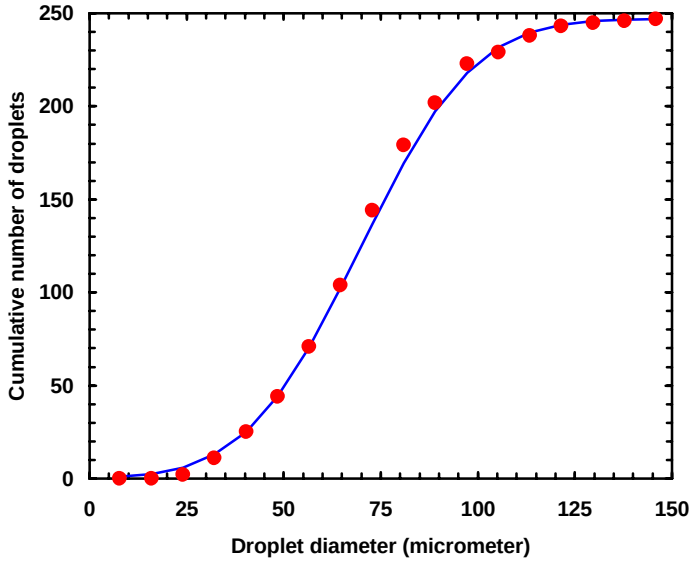


Fig. 9. The plot of the cumulative number of microdroplets and the respective normal Gaussian CDF as a function of the microdroplet diameter.

9. Conclusions

Yellow fluorescence and orange-red lasing images of a dense water spray containing Rhodamine 6G dye are used for microdroplet identification and the analysis of microdroplet size distribution. The large microdroplets are distinguished easily, since the lasing is only attainable in the large microdroplets. This technique is of limited use for aerosols, which

#1652 - $15.00 US
Received September 03, 2002; Revised October 02, 2002
(C) 2002 OSA

have small microdroplets with diameters on the order of a micrometer. Small microdroplets have few MDR's with small quality factors, and thus are unable to support lasing. Because the temporal resolution is defined by the input laser pulse duration (15 ns), this technique is well suited to the study of rapid injection events. The microdroplet size distribution obtained from the spray compares favorably with the normal Gaussian size distribution. With the proper adaptations, this technique might be used for the design and characterization of new nozzles and other spray delivery equipment in various industries.

Acknowledgments

We would like to acknowledge many helpful discussions with Prof. Derin N. Ural of Istanbul Technical University for the statistical analysis of the microdroplet size distribution data. We would also like to acknowledge the partial support of this research by the EOARD Grant No: F61775-01-WE062 and the Scientific and Technical Research Council of Turkey (TUBITAK) Grant No: TBAG-1952.

#1652 - $15.00 US Received September 03, 2002; Revised October 02, 2002
(C) 2002 OSA